Design, Fabrication, and Characterization of a Piezoelectric AFM Cantilever Array

M. Bulut Coskun, Marzieh Baan, Afshin Alipour, and S. O. Reza Moheimani

Abstract— **Atomic force microscope (AFM) is a powerful instrument, which has been successfully employed in a myriad of applications from imaging to lithography, over the last decades. Despite its widespread use, low throughput of the AFM remains one of its major limitations along with slow scan rates in tapping mode. In this work, we propose a microfabricated cantilever array composed of five cantilevers, each equipped with on-chip piezoelectric displacement sensors and an actuator for parallel imaging in tapping mode. The cantilevers are designed to have separate resonance frequencies in order to effectively minimize the vibrational coupling. The measured resonance frequencies range from 85.34 kHz to 107.78 kHz, and more than 5 kHz resonant frequency separation is achieved in the neighboring cantilevers. Vibrational coupling is mitigated by over two orders of magnitude compared to arrays with identical cantilevers. The common feedthrough problem in this type of active system is addressed by configuring the displacement sensors differentially. Finally, one of the cantilevers in the array is successfully employed for tapping mode AFM imaging.**

I. Introduction

Over the years, atomic force microscopy (AFM), has demonstrated a great potential in a variety of applications [1]–[3]. Among the different operation modes of AFM, tapping mode (TM) has been especially preferred over others, when dealing with delicate samples. In a typical TM-AFM operation, a microcantilever with a sharp tip is excited to oscillate close to its first resonance frequency by a piezoelectric shaker, and is brought in intermittent contact with the sample surface. As the cantilever is scanned over the surface, the amplitude and frequency of oscillation alter due to the change in the topography. Based on the modulation technique, the amplitude or frequency of oscillation is kept constant by a Z-positioner driven by a PI controller, which adjusts the distance between the cantilever and the sample. This well-established method has been employed to measure the mechanical, electrical and chemical quantities, manipulate the matter at micro/nanoscales and many other applications in air and liquid environments.

Despite its widespread use and advantages, throughput and scan speed of the conventional TM-AFM have remained limited over the years. One of the practical ways to increase achievable throughput is to replace the single AFM probe with an array of cantilevers. To date, a number of array configurations are proposed to reach this goal for both static and dynamic mode AFM operations [4]–[9]. Such arrays can be easily composed of tens or even hundreds of cantilevers. Regardless of the operation mode, it is highly desirable and practical for each cantilever in the array to have self-sensing and actuation capabilities, which would otherwise require separate laser/photodiode for displacement sensing, a base shaker for actuation, and a Z-positioner for each cantilever. Importantly, on-chip transducers also provide a cleaner frequency response compared to base shaker actuated conventional systems, and enable a more accurate system identification [10] for control applications. However, there are also significant challenges towards the implementation of active cantilever arrays for dynamic parallel operation.

Mechanical crosstalk among the cantilevers is a significant problem in the array configurations, especially when cantilevers operate in dynamic mode, and have close or identical resonant frequencies [11]. In this mode, cantilevers anchored to the same substrate are simultaneously driven near their first resonances. Vibration of the cantilevers transmit to the adjacent cantilevers through the substrate, and causes secondary, tertiary and even higher order mechanical couplings, rendering the use of arrays in high precision applications impractical. On the other hand, electrical feedthrough from the actuation signal to the sensor output of each cantilever has the effect of altering the resonance dynamics, which results in a drastic decline in the dynamic range. While these problems were partially addressed for single active cantilever configurations, fully operational cantilever arrays for TM operation are highly limited in the literature.

In this work, we address the mechanical crosstalk, and electrical feedthrough problems by using a piezoelectric cantilever array composed of five cantilevers each equipped with a piezoelectric actuator, and two displacement sensors. The vibrational cross-coupling problem is mitigated by over two orders of magnitude by: (1) designing the cantilevers with different dimensions in order to separate their resonance frequencies, (2) having sufficient cantilever separation, and (3) inclusions of grooves among the cantilevers on the substrate. Moreover, the common electrical feedthrough is mitigated by our previously demonstrated differential configuration for active microcantilevers [12], [13]. System identification is done for one of the cantilevers in the array, and later the same cantilever is successfully employed for tapping mode imaging using the on-chip elements.

The authors are with the Department of Mechanical Engineering, University of Texas at Dallas, Richardson, TX 75080 USA (e-mail: bulut.coskun@utdallas.edu; marzieh.baan@utdallas.edu; afshin.alipour@utdallas.edu; reza.moheimani@utdallas.edu).

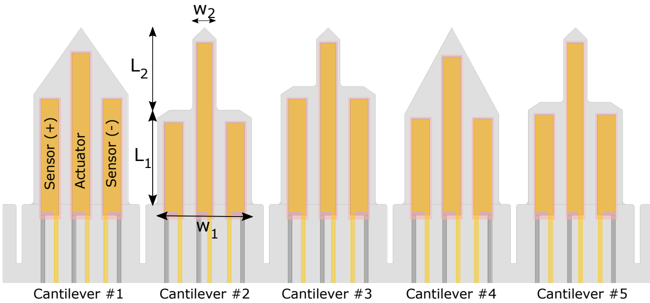

Fig. 1. A schematic of the piezoelectric cantilever array.

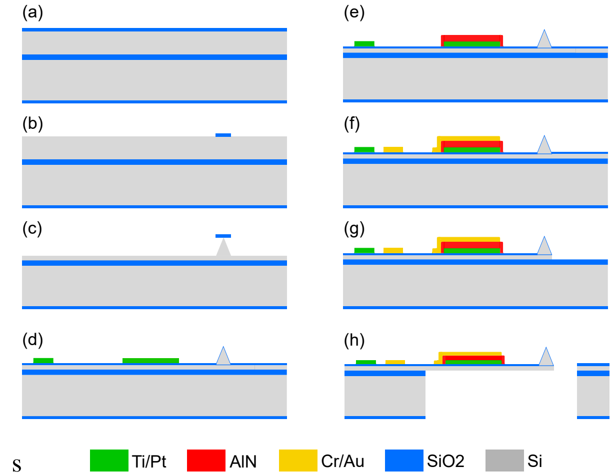

Fig. 2. Microfabrication steps: (a) PECVD Oxide deposition, (b) Dry etching of oxide to define the tip mask, (c) isotropic etch of Si via RIE (d) sputtering of the bottom electrodes (Ti / Pt) and lift-off, (e) AlN sputtering and etching, (f) deposition of the top electrodes (Cr/Au) by E-beam evaporation, and lift-off (g) RIE and DRIE etching of the thermal oxide and Si device layer (h) Backside etching and release of the array.

II. Design and Microfabrication of the Cantilever Array

The cantilevers in the array are designed in different geometries using CoventorWare software package in order to separate their resonant frequencies, and correspondingly to minimize vibrational cross-coupling during parallel tapping mode AFM operation. The resonant frequencies of the cantilevers range from 85.34 kHz to 107.78 kHz, and more than 5 kHz resonant frequency separation is achieved between the neighboring cantilevers. Cantilever dimensions along with their resonant frequencies are summarized in Figure 1 and Table 1. Each of the five cantilevers contains three parallel piezoelectric transducers, where the longer piezoelectric element in the middle and the other two on the sides are employed for actuation, and displacement sensing, respectively. The displacement sensors are configured differentially in each cantilever in order to reduce the common-mode noise, as well as mitigate the electrical feedthrough from the actuation signal to the sensor output. The details regarding the mechanical crosstalk and the electrical feedthrough mitigation are explained in the following sections.

The cantilever array is fabricated using standard cleanroom processes. In contrast to our previous process flow in [12]–[14], the probe tips are now integrated with the MEMS batch fabrication process. The AFM array is fabricated using an n-type <1 0 0> SOI wafer with 450-μm-thick handle layer, 1-μm-thick buried oxide (BOX) layer and 15-μm-thick Si device layer.

The fabrication process starts with the deposition of a 500-nm-thick SiO_2 layer via Plasma-enhanced chemical vapor deposition (PECVD) (Figure 2(a)). After that, the circular tip mask is patterned by lithography, and the oxide layer is etched via reactive ion etching (RIE) down to the device layer (Figure 2(b)). Using the circular tip features as hard mask, silicon device layer is anisotropically etched. As the etch continues, the resulting structure gradually starts to resemble an hour-glass shape, and the RIE etch is stopped, right before the circular caps fall down, when the radius of the narrow neck gets below 0.5 μm (Figure 2(c)). At this point, the wafer is placed in oxidation furnace at 950 ^0C for 210 min. During the wet oxidation, the circular caps fall down as the silicon neck is consumed, and the apex of the tips are then formed. Next, the oxide layer grown during the oxidation process is removed by Buffered Oxide Etch (BOE 7:1). Another oxide layer with 140 nm thickness is grown which will electrically insulate the upcoming top and bottom electrode layers. Finally, the tips are covered by a 10-nm-thick Cr layer in order to protect the oxide on the tips against wet etchants in the future steps.

After the tips are formed, bottom electrode features (15 nm / 150 nm-thick Ti/Pt) are deposited by sputtering and lifted off (Figure 2(d)). Next, a 750-nm-thick AlN is sputtered, and a 250 nm SiO_2 is deposited by PECVD. The

TABLE I
Summary of the cantilever design parameters and measured resonance frequencies

Cantilever	# 1	# 2	# 3	# 4	# 5
$L_1(\mu m)$	260	225	290	240	255
$w_1(\mu m)$	240	240	240	240	240
$L_2(\mu m)$	180	215	150	200	185
$w_2(\mu m)$	-	60	60	-	60
$f_{res}(kHz)$	85.34	107.78	98.29	92.85	102.39

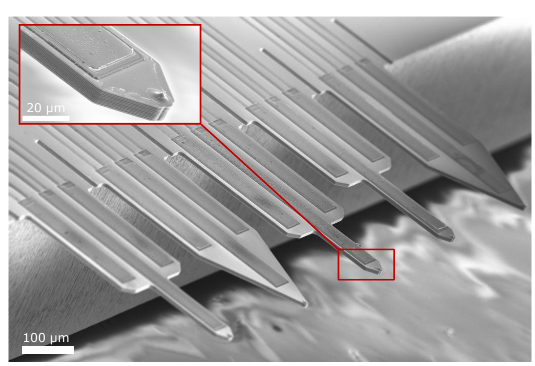

Fig. 3. SEM image of the microfabricated cantilever array.

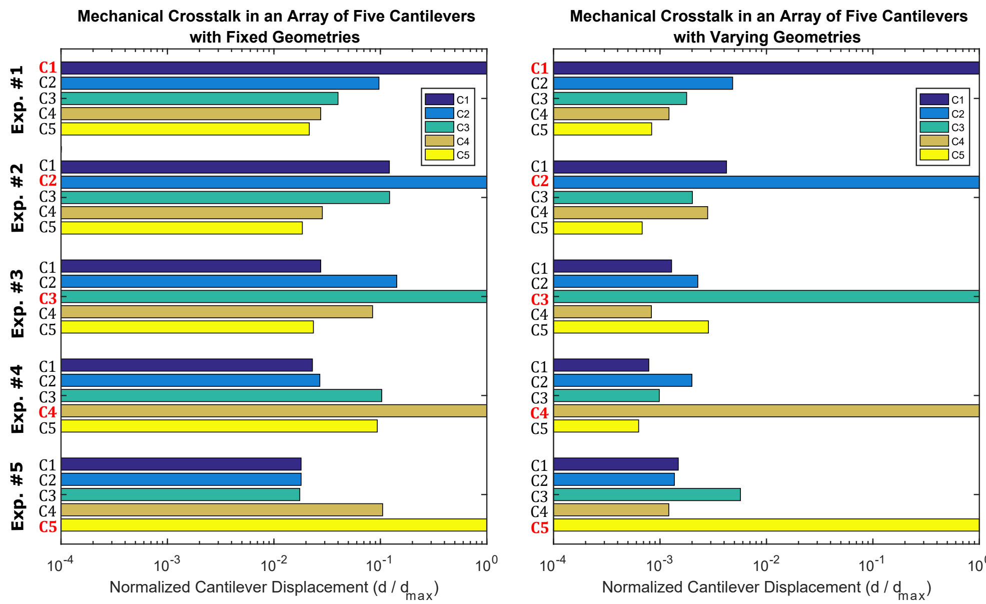

Fig. 4. Comparison of the mechanical crosstalk in: (a) an array comprised of identical cantilevers, (b) in our proposed array

PECVD layer is patterned and etched, and used as an hard mask for wet etching of the AlN layer. AlN is etched by a 2.5 % Tetramethylammonium hydroxide (TMAH) solution at 80 ^0C for about 45 s (Figure 2(e)). Next, the oxide hard mask is removed, and the top layer features (15 nm / 500 nm-thick Cr/Au) are sputtered, and lifted off (Figure 2(f)). The cantilever array shapes are patterned, and etched down to the box layer by deep reactive ion etching (DRIE) (Figure 2(g)). To release the cantilever array, the wafer is flipped, and backside etch mask patterns are transferred. The oxide layer, Si handle layer and the BOX layers are etched by RIE, DRIE and RIE processes, respectively (Figure 2(h)). The wafer is cleaned by O_2 Plasma for 10 minutes and the array is glued on and wirebonded to a PCB for characterization. A scanning electron microscope (SEM) image of the microfabricated device is shown in Figure 3.

III. Experimental Characterization

A. Experimental Investigation of the Mechanical Crosstalk

The magnitude of the mechanical crosstalk becomes substantially larger when closely spaced cantilevers with identical resonant frequencies are employed in the array. To demonstrate the severity of this case in a clear way, a series of experiments are conducted using a test array, which consists of five identical cantilevers with a resonant frequency of 48 kHz. In this experiment, a laser doppler vibrometer (LDV) is employed to apply a sinusoidal actuation signal to the on-chip piezoelectric actuator of a single cantilever at a time. While the excited cantilever oscillates at a free-air amplitude of 200 nm, the effect of the vibrational cross-coupling on the unactuated adjacent cantilevers are measured by the LDV in terms of displacement. This experiment is repeated for five times, and in each test a different cantilever is excited alone, while others remain in their rest position. Results indicate that, immediately adjacent cantilevers are significantly affected by the mechanical cross-coupling and oscillates at a free-air amplitude of above 20nm, which corresponds to 10% of the main actuation. The effect of cross-coupling decreases on the second and third adjacent cantilevers and yields a 2% coupling. Very importantly, since all the cantilevers would be simultaneously excited during an actual scan, the mechanical cross-coupling would be signifcantly larger than this experimental scenario.

Next, our proposed array is tested under the same conditions and test procedures. As shown in Figure 4, the mechanical crosstalk is subtantilaly mitigated compared to the test array, and more than two orders of magnitude of reduction is achieved.

B. Frequency Response of the Array and Feedthrough Cancellation

In order to obtain the frequency response of each of five cantilevers from the input voltage to the output of the readout circuit, differential output of the on-chip displacement sensors is obtained by a Zurich Instruments HF2LI lock-in amplifier. Here, each cantilever is driven separately by a sine-sweep signal with a 100 mV amplitude over a frequency range around the resonance frequency. The resulting cantilever frequency responses are shown in Figure 5 in blue. While the dynamic range in the frequency responses are relatively high, thanks to the differential configuration, the presence of a zero in the vicinity of the pole near the resonance of each cantilever indicates that the electrical feedthrough is not fully mitigated. In order to maximize the level of feedthrough reduction, for each cantillever, a tunable gain is implemented right after one of the sensor outputs, and prior to the differential amplifier in the readout circuit. By adjusting the gain, when the differential sensor output levels are matched, a phase of -90 degrees is achieved, and the level of feedthrough cancellation is maximized. As shown in

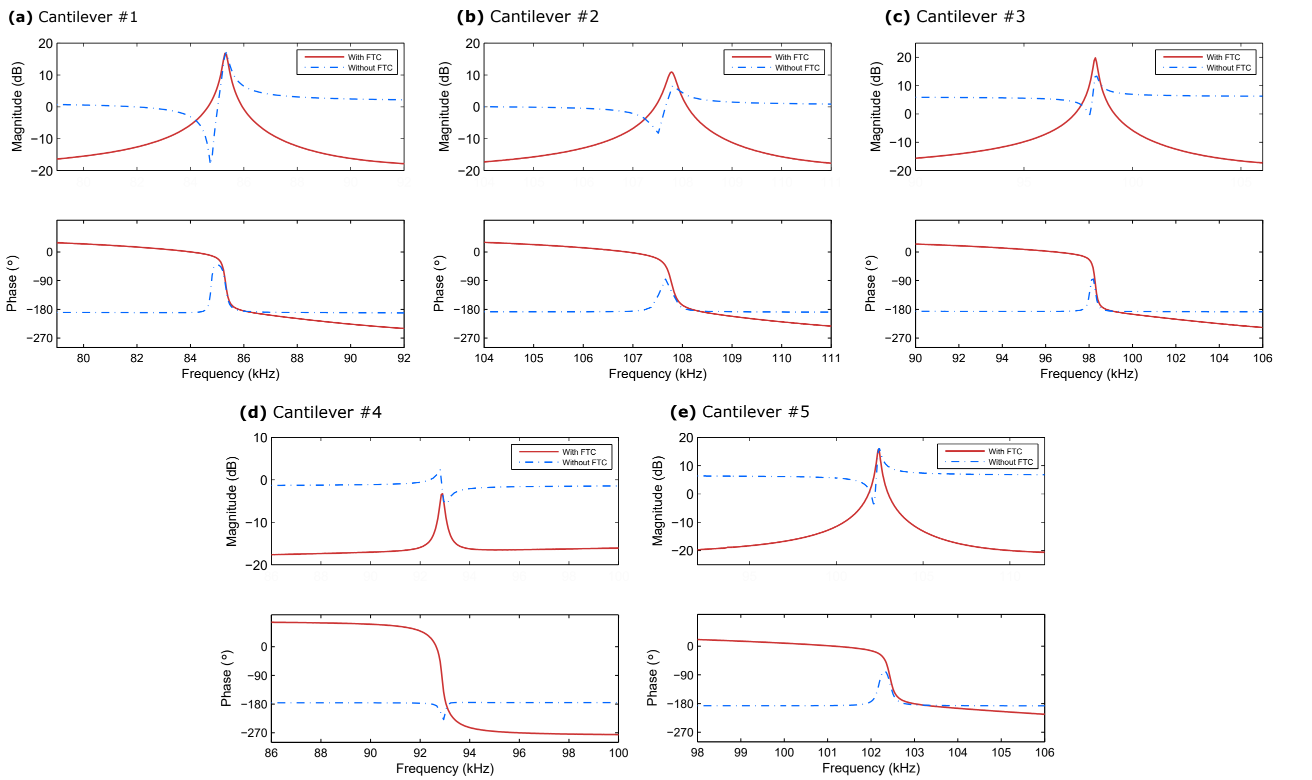

Fig. 5. (a-e) Frequency response of the cantilevers #1-5 from the actuation voltage to the sensor readout circuit output before and after the feedthrough cancellation (FTC).

Figure 5 in red, the dynamic range at the first resonance of each cantilever reaches over 30 dB. More details regarding the readout circuit and electrical feedthrough cancellation can be found in [12].

C. System Identification

After the feedthrough is cancelled and the dynamics of the cantilever are revealed, the open-loop transfer function of Cantilever #2 is identified from the actuation voltage to the sensor output. While this type of systems usually can be represented by a second-order transfer function, the remaining electrical feedthrough originating from the chip body, routing, bonding pads, cables and the readout circuit necessitates inclusion of an extra pole and zeros to the transfer function to model the system accurately. As shown in Figure 6, a biproper third order transfer function is fitted to the feedthrough-compensated frequency response using the least squares method within the frequency range of 104 kHz to 111 kHz, in order to model the first resonance of the cantilever as:

$$G(s) = \frac{1.828s^3 + 3.097 \times 10^5 s^2 + 8.341 \times 10^{11} s + 1.820 \times 10^{17}}{s^3 + 1.388 \times 10^7 s^2 + 4.754 \times 10^{11} s + 6.364 \times 10^{18}}. \quad (1)$$

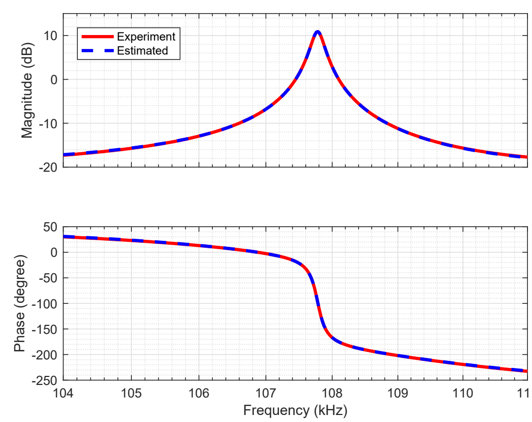

Fig. 6. Frequency response of the cantilever #2 together with the identifed model.

IV. AFM Imaging

A. Experimental Setup

For the imaging experiments, the second cantilever in the array is used along with the embedded components of a commercially available AFM (AFMWorkshop TT-AFM). First, the array chip is mounted on a carrier PCB, which has connections to the readout board containing the readout electronics for the differentially configured on-chip displacement sensors, as well as the ports for the cantilever excitation. The carrier PCB is then mounted on a 3D printed part which is then assembled to the probe holder of the commercial AFM.

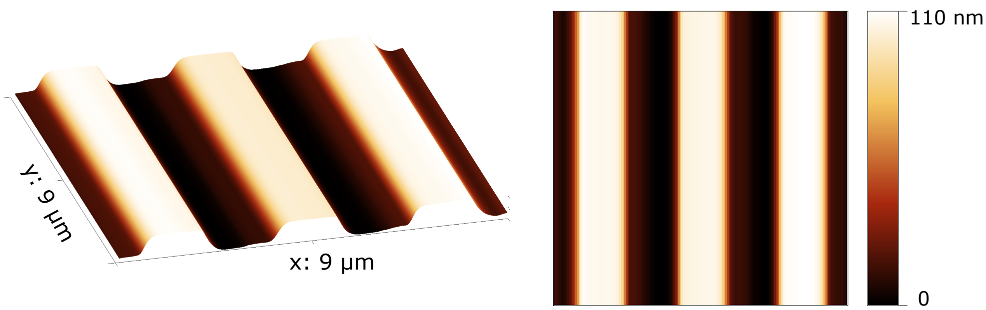

Fig. 7. 3D and 2D AFM images of the calibration grating obtained by Cantilever #2.

Here, the base shaker and photodetector of commercial AFM are electronically bypassed by the on-chip transducers of the cantilever. Otherwise, the scanning operation and imaging are done by the built-in components of the AFM and its associated software.

B. Imaging

Cantilever #2 is employed to obtain the images of a calibration sample (NT-MDT TGZ), containing repeating $110 \pm 2\,nm$ high rectangular steps with a period of $3.00 \pm 0.05\,\mu m$. Prior to the imaging, the cantilever is excited at its resonance with an actuation voltage of 100 mV in order to achieve a free-air amplitude of 200 nm, which is previously validated by the laser doppler vibrometer. Using the commercial AFM, the cantilever is approached to the surface in order to reach the set amplitude which is adjusted to be around 60% of the free-air amplitude. The scan rate and the scan area are set to 1 Hz, and $9\,\mu m \times 9\,\mu m$, respectively.

The resulting 3D, and 2D topography images are shown in Figure 7. The images are postprocessed by Gywddion using standard built-in tools, namely, mean plane substraction, row alignment and polynomial background removal.

V. Conclusion and Future Work

In conclusion, we have demonstrated the design, fabrication, and characterization of an AFM cantilever array designed for parallel scanning operation. The array comprises five piezoelectric cantilevers with on-chip sensing and actuation capabilities that provide certain advantages including, cleaner frequency response, rapid and straightforward feedthrough cancellation, and bypassing of the bulky shaker and laser/photodiode which exist in conventional systems. Importantly, each cantilever is mechanically designed to have a separate resonant frequency in order to drastically minimize the vibrational coupling during the TM operation. We have employed the second cantilever of the array for taping mode imaging and sucessfully obtained the surface topography of a commercially available calibration sample.

Future work will focus on parallel imaging using the array. Reaching this goal necessitates implementing separate Z-axis actuation on each cantilever. This can be achieved by simultaneously applying the excitation signal at resonance frequency and a DC bias which is fed by the Z-axis controller output.

Acknowledgements

This material is based upon work supported by the U.S. Department of Energy's Office of Energy Efficiency and Renewable Energy (EERE) under the Advanced Manufacturing Office Award Number DE-EE0008322. Facilities provided by the University of Texas at Dallas Cleanroom Research Laboratory were used to fabricate this device.

Disclaimer

This report was prepared as an account of work sponsored by an agency of the United States Government. Neither the United States Government nor any agency thereof, nor any of their employees, makes any warranty, express or implied, or assumes any legal liability or responsibility for the accuracy, completeness, or usefulness of any information, apparatus, product, or process disclosed, or represents that its use would not infringe privately owned rights. Reference herein to any specific commercial product, process, or service by trade name, trademark, manufacturer, or otherwise does not necessarily constitute or imply its endorsement, recommendation, or favoring by the United States Government or any agency thereof. The views and opinions of authors expressed herein do not necessarily state or reflect those of the United States Government or any agency thereof.

References

[1] S. Krämer, R. R. Fuierer, and C. B. Gorman, "Scanning probe lithography using self-assembled monolayers," *Chemical Reviews*, vol. 103, no. 11, pp. 4367–4418, 2003.

[2] Y. H. Guu, "AFM surface imaging of AISI D2 tool steel machined by the EDM process," *Applied Surface Science*, vol. 242, no. 3, pp. 245–250, 2005.

[3] M. Göken and M. Kempf, "Microstructural properties of superalloys investigated by nanoindentations in an atomic force microscope," *Acta Materialia*, vol. 47, no. 3, pp. 1043–1052, 1999.

[4] S. C. Minne, S. R. Manalis, and C. F. Quate, "Parallel atomic force microscopy using cantilevers with integrated piezoresistive sensors and integrated piezoelectric actuators," *Applied Physics Letters*, vol. 67, no. 26, pp. 3918–3920, 1995.

[5] S. C. Minne, G. Yaralioglu, S. R. Manalis, J. D. Adams, J. Zesch, A. Atalar, and C. F. Quate, "Automated parallel high-speed atomic force microscopy," *Applied Physics Letters*, vol. 72, no. 18, pp. 2340–2342, 1998.

[6] A. Ahmad, N. Nikolov, T. Angelov, T. Ivanov, A. Reum, I. Atanasov, E. Guliyev, V. Ishchuk, M. Kaestner, Y. Krivoshapkina, S. Lenk, C. Lenk, I. W. Rangelow, and M. Holz, "Large area fast-afm scanning with active quattro cantilever arrays," *Journal of Vacuum Science Technology B*, vol. 34, no. 6, p. 06KM03, 2016. [Online]. Available: https://doi.org/10.1116/1.4967159

[7] R. Fasching, Y. Tao, and F. Prinz, "Cantilever tip probe arrays for simultaneous secm and afm analysis," *Sensors and Actuators B: Chemical*, vol. 108, no. 1, pp. 964 – 972, 2005, proceedings of the Tenth International Meeting on Chemical Sensors. [Online]. Available: http://www.sciencedirect.com/science/article/pii/S0925400504007968

[8] P. Vettiger, M. Despont, U. Drechsler, U. Durig, W. Haberle, M. I. Lutwyche, H. E. Rothuizen, R. Stutz, R. Widmer, and G. K. Binnig, "The millipede-more than thousand tips for future afm storage," *IBM Journal of Research and Development*, vol. 44, no. 3, pp. 323–340, May 2000.

[9] M. Lutwyche, C. Andreoli, G. Binnig, J. Brugger, U. Drechsler, W. HÃ€berle, H. Rohrer, H. Rothuizen, P. Vettiger, G. Yaralioglu, and C. Quate, "5x5 2d afm cantilever arrays a first step towards a terabit storage device," *Sensors and Actuators A: Physical*, vol. 73, no. 1, pp. 89 – 94, 1999. [Online]. Available: http://www.sciencedirect.com/science/article/pii/S0924424798002593

[10] M. G. Ruppert and S. O. R. Moheimani, "High-bandwidth multimode self-sensing in bimodal atomic force microscopy," *Beilstein Journal of Nanotechnology*, vol. 7, no. 1, pp. 284–295, 2016.

[11] T. Sulzbach, W. Engl, R. Maier, and P. Besmens, "Individual addressable cantilever arrays for parallel atomic force microscope," *Nanotechnology*, pp. 378–381, 2010.

[12] M. B. Coskun, A. G. Fowler, M. Maroufi, and S. O. R. Moheimani, "On-chip feedthrough cancellation methods for microfabricated AFM cantilevers with integrated piezoelectric transducers," *Journal of Microelectromechanical Systems*, 2017.

[13] M. B. Coskun, H. Alemansour, A. G. Fowler, M. Maroufi, and S. O. R. Moheimani, "q control of an active afm cantilever with differential sensing configuration," *IEEE Transactions on Control Systems Technology*, pp. 1–8, 2018.

[14] A. G. Fowler, M. B. Coskun, and S. O. R. Moheimani, "Q control of a microfabricated piezoelectric cantilever with on-chip feedthrough cancellation," in *2017 IEEE Conference on Control Technology and Applications (CCTA)*, Aug 2017, pp. 123–128.